Int J Mater Form (2009) Vol. 2 Suppl 1:383–386
DOI 10.1007/s12289-009-0459-z

NUMERICAL SIMULATION OF FRICTION STIR WELDING PROCESS

Dongun Kim[1], Harsha Badarinarayan[2], Ill Ryu[1], Ji Hoon Kim[3], Chongmin Kim[4], Kazutaka Okamoto[5], R. H. Wagoner[3], Kwansoo Chung[1,*]

[1]Department of Material Science and Engineering, Seoul National University
[2]Research and Development Division, Hitachi America Ltd.
[3]Department of Materials Science and Engineering, The Ohio State University
[4]Materials and Process Lab., R&D Center & NAO Planning, General Motors Corporation
[5]Hitachi Research Laboratory, Hitachi Ltd.

ABSTRACT: Thermo-mechanical simulations of the friction stir butt welding and friction stir spot welding processes were performed for AA5083-H18 sheets, utilizing commercial FVM codes which are based on the Eulerian formulation. For the friction stir butt welding process, the computational fluid dynamics code, STAR-CCM+, was utilized under the steady state condition. Temperature and strain rate histories along the material flow were calculated and simulated temperature distributions (profiles and peak values) were compared with experiments for verification. It was found that by including proper thermal properties of the backing plate (anvil) the accuracy of the simulation results increased significantly. For the friction stir spot welding process, the computational fluid dynamics code, STAR-CD, was utilized under the unsteady condition to understand the effect of pin geometry on material flow and weld strength.

KEYWORDS: Friction stir butt welding, Friction stir spot welding, Thermo-mechanical Simulation, AA5083-H18

1 INTRODUCTION

In this report, simulations of the friction stir butt welding (FSBW) as well as friction stir spot welding (FSSW) processes were performed utilizing Eulerian Computational Fluid Dynamics codes, STAR-CCM+ [1] and STAR-CD [2]. Thermo-mechanical simulations were carried out for AA5083-H18 as a coupled analysis along with the user subroutine to define temperature dependent material properties. As for the FSBW case, the process, consisting of plunging, short dwell, long linear welding and retracting steps, was simplified as a steady state process wherein the process achieves an equilibrium operating temperature in a relatively short time [3]. As for the FSSW case, the process consists of plunging, short dwelling and retracting steps. Unlike the FSBW process, the FSSW cannot be considered as a steady state process wherein the whole welding process is conducted in a short time as well as consists of a short dwelling step. Simulations were directly verified for temperature history in the case of FSBW but indirectly for spot weld strength in the FSSW case.

2 THEORY

In order to calculate the temperature distribution and plastic deformation during FSW Process, continuity and momentum equation as well as energy equation are solved with temperature dependent or temperature and strain rate dependent material properties. The constitutive law (for the mechanical strain) is assumed rate-insensitive and incompressible rigid-perfect Mises plastic using the normality rule,

$$\mathbf{S} = 2\mu\mathbf{D} \;\; and \;\; \mathbf{D} = \dot{\bar{\varepsilon}}\frac{\partial\bar{\sigma}}{\partial\mathbf{S}} = \frac{3\dot{\bar{\varepsilon}}}{2\bar{\sigma}}\mathbf{S} = \frac{\mathbf{S}}{2\mu}$$
$$\bar{\sigma} = \sqrt{\frac{3}{2}\mathbf{S}\cdot\mathbf{S}} \;\; and \;\; \dot{\bar{\varepsilon}} = \sqrt{\frac{2}{3}\mathbf{D}\cdot\mathbf{D}} \qquad (1)$$

where **D** and **S** are the rate of deformation tensor and the deviatoric stress tensor, and $\bar{\sigma}$, $\dot{\bar{\varepsilon}}$ and μ are the Mises effective yield stress, effective strain rate and the viscosity. The yield stress is temperature dependent property and the viscosity is temperature and strain rate dependent property, given by eq. (2)

$$\mu = \frac{\bar{\sigma}}{3\dot{\bar{\varepsilon}}} \qquad (2)$$

a baffle heat transfer boundary condition was applied, in which the relation between the heat flow rate across the contact boundary with an area A is given by

$$\tilde{q} = -kA\frac{dT}{dn} \approx -\frac{\Delta T}{R} \qquad R = \sum_i^n \frac{\Delta n_i}{k_i A} \qquad (3)$$

* Corresponding author: Address: 33-214, San 56-1, Shillim-Dong, Gwanak-Gu, Seoul 151-742, Korea
Phone: 82-2-880-7189, Fax: 82-2-885-1748 and Email: kchung@snu.ac.kr

where k_i and Δn_i are the thermal conductivity and thickness, respectively, of the i-th layer comprising the contact boundary and R is a representative thermal resistance for the area A (here, the n-direction is normal to the boundary surface). Eq. (3) is derived under the condition that the heat flow rate is maintained for each layer comprising the contact boundary.

3 EXPERIMENTS

3.1 FSBW

FSBW was performed on AA5083-H18 sheets by using a CNC controlled 3-D FSW system "Hitachi GR-3DM10T" with 11 KW spindle servomotor, as shown in Figure 1 [4].

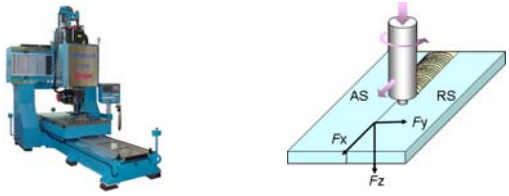

Figure 1: *CNC controlled 3-D FSW system "Hitachi GR-3DM10T" with 11 KW spindle servomotor and description for the welding process.*

The anvil upon which the work-piece is laid for welding was made of a low carbon steel 1020, while the tool was made of tool steel H13 with the shoulder and pin diameters of 10 mm and 4 mm, respectively. The shoulder had a concave profile which acts as an escape volume for the material displaced by the pin, while preventing the material from extruding out of the sides of the shoulder and maintaining downward pressure. The pin is right-hand threaded. The pin length is slightly less than the thickness of work-pieces, with 1.34 mm for AA5083-H18 (sheet thickness of 1.64 mm). The welding tool was tilted at an angle of 3 degree from the normal direction of the work sheets towards the trailing side of the tool. Three welding conditions were tried out: 1,000 rpm/100 mm/min, 1,000 rpm/300 mm/min and 1,500 rpm/150 mm/min (=rotational/linear translational speed).

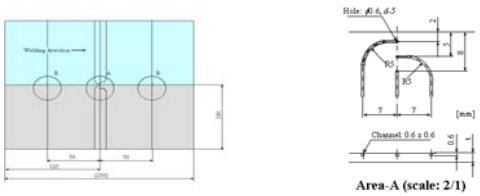

Figure 2: *Schematic illustration of thermocouple placement.*

As shown in Figure 2, for measuring temperature in the regions near the top surface, three small channels, into which sheathed K-type thermocouples were placed, were machined from the sheet bottom surface up into the sheet by 1.04 mm. The tip of the thermocouples was located 2 mm, 5 mm, and 8 mm away from the weld seam line, respectively. All the temperature measurements were made on the advancing side as well as retreating side of welds.

3.2 FSSW

FSSW was performed on AA5083-H18 (sheet thickness of 1.64mm-upper one and 1.24 mm-lower one) sheets by using a CNC controlled 3-D Linear FSW system "HitSpin type GR3DC5T" with 7.5 KW spindle servomotor, as shown in Figure 3.

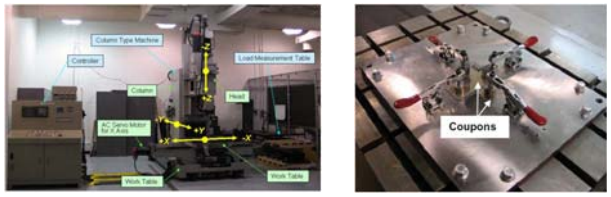

Figure 3: *CNC controlled 3-D linear FSW system 'HitSpin type GR3DC5T' and welding jig with a coupon in a cross-tension configuration.*

Welds were made in a cross-tension configuration with coupon dimensions being 150 mm x 50 mm, as shown in Figure 3 with the jig used for welding [5]. Since the purpose of this study was to evaluate the effect of tool geometry on static strength, the weld parameters were fixed as follows: the tool rotation speed was 1,500 rpm, while the plunge and retract speed was 20 mm/min and the dwell time was 2 seconds.
Cross sectional macro- and micro-structures of welds were examined by using an optical microscope for AA5083-H18 sheet. The specimens were also tested for weld strength on an Instron screw driven test machine at a constant crosshead speed of 5mm/min. [6]

4 SIMULATIONS

4.1 FSBW

The thermo-mechanical simulation of the FSBW process for AA5083-H18 was performed using the CFD code, STAR-CCM+ [1]. Dimensions of the model are shown in Figure 4. The work-piece is 200 mm x 600 mm x 1.64 mm in thickness which lies on an anvil with similar dimensions but with the thickness of 10mm. The radii of the pin and the tool shoulder were 2 mm and 5 mm, respectively. The pin length was 1.34 mm from the tool shoulder edge and the plunging depth of the tool shoulder edge was 0.2 mm. The concavity of the shoulder was 10 degrees and the tool was tilted at an angle of 3 degrees in the trailing direction of the weld line.

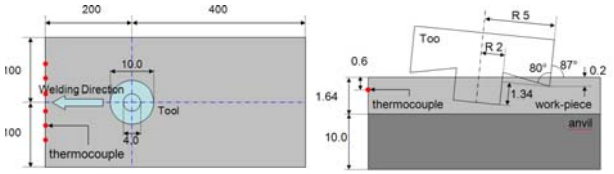

Figure 4: *Dimensions of the thermo–mechanical model: top view and section view of the tool (in mm).*

The rate-insensitive and incompressible rigid-perfect Mises plastic property was applied for the work-piece as described in Section 2. Temperature dependent yield

stresses for AA5083-H18 were used in this work, as shown in Table 1. As for thermal properties, only the room temperature data was available for AA5083-H18 and their temperature dependent properties were not available. Therefore, assumed temperature dependent properties were obtained from those of AA5052-H32 [7] by proportionally modifying the values considering the ratios at room temperature values of the two materials, as shown in Table 2. And constant thermal properties were implemented for anvil material with Low Carbon Steel 1020, as shown in Table 3 [8].

Table 1: *Temperature dependent yield stress*

Temp.(°C)	Y.S.(MPa)
20	440
100	437
200	364
300	181
400	61
440	50
540	40
570	0

Table 2: *Temperature dependent thermal conductivity, specific heat and density of AA5083-H18*

Temp. (°C)	Conductivity (W/m°C)	Specific Heat (J/Kg°C)	Density (Kg/m^3)
-20	112.5	924.1	2673.9
80	122.7	984.2	2642.7
180	131.6	1039.6	2629.4
280	142.3	1081.2	2611.5
380	152.5	1136.6	2589.3
480	159.5	1178.2	2567.0
580	177.2	1261.4	2549.2

Table 3: *Material properties of Low Carbon Steel 1020 at room temperature*

Conductivity (W/m°C)	Specific Heat (J/Kg°C)	Density (Kg/m^3)
51.9	486.0	7,850.0

As for the heat equation, the convective heat transfer coefficient of 30 W/m^2°C was used for the top and sides of the work–piece, which is typical for natural convection heat transfer between aluminum and air [9]. The baffle heat transfer boundary condition was placed with one layer each for the work-piece and the anvil. Also, the convective heat transfer coefficient of 35 W/m^2°C was used for the sides of the anvil which is typical for natural convection heat transfer between steel and air [10]. At the bottom of the anvil, the coefficient was assumed 200 W/m^2°C. Heat transfer at the interface between the tool and the work-piece was also ignored with the vanishing temperature gradient at the boundary.

4.2 FSSW

The thermo-mechanical simulation of the FSSW process for AA5083-H18 was performed using the CFD code, STAR-CD [2]. The FSSW process consists of tool plunging, a short dwelling and tool retracting steps. But, only the 2 second dwelling step was simulated in which the rotating tool was plunged into the work-piece in a lap configuration. Two types of pins were considered: cylindrical and triangular pins with concaved shoulders. Unlike the FSBW, the FSSW was considered as an unsteady state process. The cylindrical and triangular pins both have 10 degree concave shoulders. The pin radius was 2.5 mm and the shoulder radius was 6 mm, while the pin length was 1.6 mm from the shoulder edge and the plunge depth of the shoulder was 0.2mm. The diameter of the circle inscribed by the triangular pin was the same as the diameter of the cylindrical pin. The model description and dimensions are shown in Figure 5 with 2.88mm thickness (two work-pieces in a lab configuration were considered as one piece) with the work-piece radius of 50mm.

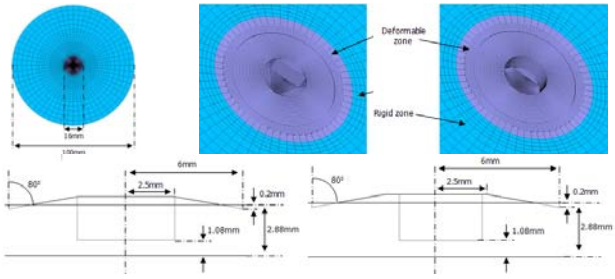

Figure 5: *Top view for cylindrical pin and triangular pin (upper), and model dimension (lower).*

The convective heat transfer coefficient of 30 W/m^2°C was used for the top and sides of the work–piece [9]. At the bottom of the work-piece, the convective heat transfer coefficient was assumed to be 2,000 W/m^2°C just below the tool considering that heat transfer between two contacting surfaces increases when the pressure between them increases under the tool [11]. For the remaining bottom surface, the coefficient was assumed 200 W/m^2°C.

5 Results

5.1 FSBW

In order to verify the numerical simulation results, the simulated temperature peak values were compared with experimental results [4] that were obtained using thermocouples at various locations along the weld path, as shown in Table 4 and Figures 6~10. The simulation results matched very closely with experiments.

Table 4: *Result summaries showing experimental and simulation result for each case.*

		Advancing Side			Retreating Side		
		2mm	5mm	8mm	2mm	5mm	8mm
1000rpm 100mm/min	Experiment	525	420	300	480	400	300
	Simulation	525	448	276	516	427	266
1000rpm 300mm/min	Experiment	460	400	205	·	·	·
	Simulation	467	401	223	459	377	206
1500rpm 150mm/min	Experiment	530	450	267	·	·	·
	Simulation	541	444	266	535	430	257

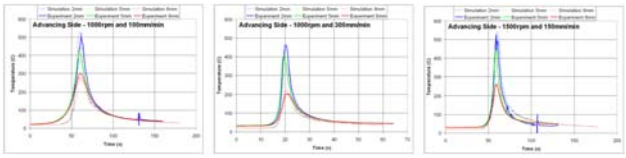

(a) (b) (c)

Figure 6: *Computed and experimental temperature history at locations away from the weld center along the width on the advancing side*

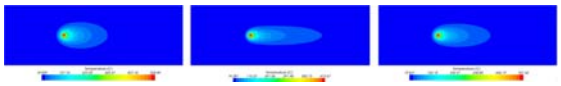

(a) (b) (c)

Figure 7: *Temperature profile at the top surface for each welding conditions*

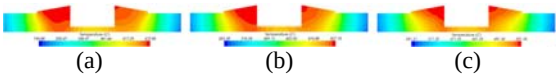

(a) (b) (c)

Figure 8: *Temperature cross section profile near the tool for each welding conditions*

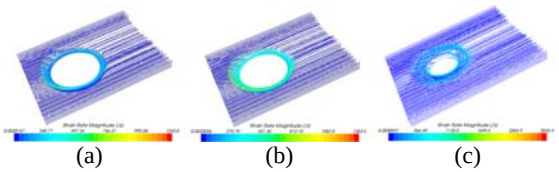

(a) (b) (c)

Figure 9: *Material flow with strain rate history for each welding conditions*

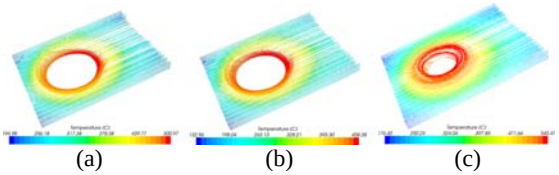

(a) (b) (c)

Figure 10: *Material flow with temperature history for (a) 1000rpm and 100mm/min, (b) 1000rpm and 300mm/min and (c) 1500rpm and 150mm/min (in °C)*

5.2 FSSW

Temperature profiles at the top surface as well as any cross section surface of sheets for the cylindrical and triangular pins were calculated at various moments. Also, material flow patterns were simulated at various instances. For the cylindrical pin, materials near the tool did not move that much along the radial direction. However, for the triangular pin, materials near the pin boundary showed significant in and out motion along the radial direction, since the boundary of the triangular pin moved in and out along the radial direction during the tool rotation. Note that heat generation of the cylindrical and triangular pins was similar, only the material flow pattern was different which then caused the static weld strength to be different. The weld strength for the concave triangular pin was almost twice as that of the concave cylindrical pin. The triangular pin geometry yielded higher weld strength compared to the cylindrical pin, since the material flow pattern affected the hook formation near the pin, as shown in figure 11 [6].

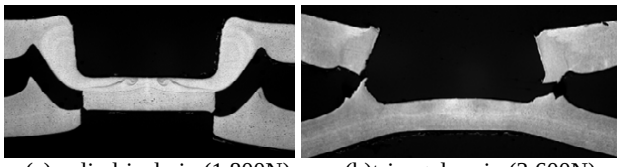

(a) cylindrical pin (1,800N) (b)triangular pin (3,600N)

Figure 11: *Sectional macrographs in the cross-tension test*

6 CONCLUSIONS

The FSBW process was solved under the steady state condition and simulated temperature results matched with experiments very closely, while nobody has achieved such an agreement of the numerical results with experiments. Above results from the simulation can be a good control group to study welds performances. In particular, the effective strain results as well as the temperature history of welds may play an important role in the decision of the grain size after welding as well as the AGG (abnormal grain growth) phenomenon, where one grain grows at a much greater rate than its neighbours, after PWHT (post weld heat treatment). As for the FSSW, simulation was conducted under the unsteady state condition to understand the tool geometry effect on weld strength. Simulated material flow pattern was discussed to explain the hook formation near the pin boundary since the hook formation is a key geometric characteristic of the weld strength.

ACKNOWLEDGEMENT

The authors of this paper would like to thank the Korea Science and Engineering Foundation (KOSEF) for sponsoring this research through the SRC/ERC Program of MOST/KOSEF (R11-2005-065).

REFERENCES

[1] CD-Adacpco, 2007. STAR-CCM+ 2.10.017.
[2] CD-Adapco, 2005. STAR-CD 3.26
[3] Badarinarayan, H., 2007. APL Effect of Tool Thermal Expansion and Durability in Friction Stir Spot Welding, Hitachi America Ltd., Internal Report
[4] Okamoto, K., Hirano, S., Inagaki, M. and Odakura, T., 2004. Friction Stir Welding of Automotive Alloy Sheets for Tailor Welded Blank, Hitachi Ltd., Internal Report
[5] Badarinarayan, H., Yang, Q. and Hunt, F., 2008a. Effect of Tool Geometry and Pin Length on Failure Mode and Static Strength of Friction Stir Spot Welds, SAE World Congress & Exhibition, SAE, Detroit, MI, USA (Paper #2008-01-0147)
[6] Badarinarayan, H., Yang, Q. and Zhu, S., 2008b. Effect of Tool Geometry on Static Strength of Friction Stir Spot Welded Aluminum Alloy, International Journal of Machine Tools & Manufacture, doi:10.1016/j.ijmachtools.2008.09.004
[7] Zhu, X.K. and Chao, Y.J., 2002. Effects of Temperature-dependent Material Properties on Welding Simulation, Computers & Structures, Vol. 80, pp. 967-976
[8] Callister Jr., W. D., 2003. Materials Science and Engineering: an Introduction 6th Ed., pp.737~758
[9] Chao, Y.J., Qi, X. and Tang, W., 2003. Heat Transfer in Friction Stir Welding-Experimental and Numerical Studies, Transactions of the ASME Vol. 125, p.138
[10] Totten, G. E., 2007. Steel Heat Treatment Handbook 2nd Ed., CRC Press, p. 567
[11] Hyoe, T., Colegrove, P. A. and Shercliff, H. R., 2003. Thermal and Microstructure Modelling in Thick Plate Aluminium Alloy 7075 Friction Stir Welds, Proceeding of TMS Spring Meeting, Friction Stir Welding II, TMS, San Diego, CA, USA